# Direct and Indirect Salt Effects on Homotypic Phase Separation

Matthew MacAinsh[1], Souvik Dey[1], Huan-Xiang Zhou[1,2,*]

[1]Department of Chemistry and [2]Department of Physics, University of Illinois Chicago, Chicago, IL 60607, USA

*Correspondence e-mail: hzhou43@uic.edu

**Abstract**

The low-complexity domain of hnRNPA1 (A1-LCD) phase separates in a salt-dependent manner. Unlike many intrinsically disordered proteins (IDPs) whose phase separation is suppressed by increasing salt concentrations, the phase separation of A1-LCD is promoted by > 100 mM NaCl. To investigate the atypical salt effect on A1-LCD phase separation, we carried out all-atom molecular dynamics simulations of systems comprising multiple A1-LCD chains at NaCl concentrations from 50 to 1000 mM NaCl. The ions occupy first-shell as well as more distant sites around the IDP chains, with Arg sidechains and backbone carbonyls the favored partners of $Cl^-$ and $Na^+$, respectively. They play two direct roles in driving A1-LCD condensation. The first is to neutralize the high net charge of the protein (+9) by an excess of bound $Cl^-$ over $Na^+$; the second is to bridge between A1-LCD chains, thereby fortifying the intermolecular interaction networks in the dense phase. At high concentrations, NaCl also indirectly strengthens π-π, cation-π, and amino-π interactions, by drawing water away from the interaction partners. Therefore, at low salt, A1-LCD is prevented from phase separation by net charge repulsion; at intermediate concentrations, NaCl neutralizes enough of the net charge while also bridging IDP chains to drive phase separation. This drive becomes even stronger at high salt due to strengthened π-type interactions. Based on this understanding, four classes of salt dependence of IDP phase separation can be predicted from amino-acid composition.

## Introduction

Biomolecular condensates formed via liquid-liquid phase separation (LLPS) mediate a variety of cellular functions such as biogenesis of the ribosome and stress response.[1,2] The driver for phase separation or condensation is intermolecular interactions, including electrostatic, hydrogen bonding, π-π, cation-π, amino-π, and hydrophobic.[3-5] Salt can tune all these interactions and thus exert significant effects on phase separation. While the screening effect of salt on electrostatic interactions is well-known, its effects on other types of interactions may be indirect and perhaps are less appreciated. In particular, high salt strengthens hydrophobic interactions by increasing the surface tension of water.[6,7] Because salt can exert disparate effects on different types of interactions, it can be used as a perturbation to dissect the relative importance of these interactions in phase separation.[8,9] Inside cells, proteins can encounter varying salt conditions at different locations or at different times, and therefore the drive for their phase separation can span a wide range.

Numerous studies of salt effects on protein phase separation have been reported. The most typical effect is the suppression of phase separation by screening electrostatic attraction, both for homotypic systems[10-17] and for heterotypic systems.[8,18] However, salt can also promote phase separation, although the mechanism is not always clear.[10,19-27] In particular, Krainer et. al.[19] observed a "reentrant" salt effect on the phase separation of five intrinsically disordered proteins (IDPs): phase separation occurs without salt, is prohibited by medium salt, and reemerges at high salt. They attributed the reemergence of phase separation to strengthened π-type and hydrophobic interactions that overcompensate weakened electrostatic attraction. A unifying understanding of how salt affects the phase separation of IDPs is still lacking. For example, it is an open question whether salt effects on phase separation can be predicted from the protein sequence. Deep knowledge, in particular at the atomic level, of how salt affects intermolecular interactions and, ultimately, phase separation is required.

The low-complexity domain of hnRNPA1 (A1-LCD) represents another IDP where an atypical salt effect was reported.[10] The full-length protein, comprising folded domains along with the LCD, phase separates in the absence of salt and the tendency to phase separate is reduced upon adding salt, thus exhibiting the typical salt effect. A screening mechanism, specifically of electrostatic attraction between the LCD and the folded domains, is supported by small-angle X-

ray scattering and coarse-grained molecular dynamics (MD) simulations. In contrast, A1-LCD does not phase separate without salt and starts to do so only after 100 mM NaCl is added. An earlier study revealed that π-types of interactions, mediated by aromatic residues, drive the phase separation of A1-LCD.[28] A follow-up study, based on charge mutations, further showed that the net charge plays a strong suppressive role.[29] The saturation concentration ($C_{sat}$) for phase separation is minimum at a net charge near 0, and increases by two orders of magnitude, signifying an enormous weakening of the drive for phase separation, when the net charge moves away from neutrality in either direction. In a more recent study, salt promoted the homotypic phase separation of both A1-LCD and FUS-LCD, but suppressed the heterotypic phase separation of their mixture.[8] The salt effect on the phase separation of A1-LCD was modeled by a Debye-Hückel potential in coarse-grained simulations.[30] Similarly, the salt effect on the phase separation of another IDP, Ddx4, was analyzed using the random phase approximation based on a coarse-grained representation.[31] Coarse-grained simulations with explicit water and ions have been used to study salt effects in both homotypic and heterotypic phase separation.[32]

All-atom MD simulations can uniquely provide mechanistic insight into the driving force and properties of biomolecular condensates.[5] For example, these simulations showed that ATP, a small molecule with a -4 charge, bridges between positively charged IDP chains in driving phase separation.[33] The intermolecular interactions quickly break and reform, explaining why the condensates can rapidly fuse despite very high macroscopic viscosity. Similarly, quick breakup and reformation of salt bridges in a heterotypic condensate allow the protein molecules to be extremely dynamic in a highly viscous environment.[18] Recently, all-atom MD simulations provided explanations for wide variations in phase equilibrium and material properties among condensates of tetrapeptides with different amino-acid compositions.[34] These and other simulations[35] show that all attractive residue-residue contacts contribute to the drive for phase separation.

Here we study salt effects on A1-LCD condensation by all-atom MD simulations. The simulations reveal two direct effects and one indirect effect of NaCl: neutralization of net charge and bridging between protein chains as well as strengthening of π-type interactions by drawing water away from the interaction partners. We also present a unified picture of salt dependences of

phase separation by defining four distinct classes and predict these classes from amino-acid composition.

## Results

### Salt condenses A1-LCD and increases inter-chain interactions

The 131-residue A1-LCD is comprised mostly of Gly and Ser (51 and 22, respectively), followed by 18 aromatic residues (11 Phe and 7 Tyr), 17 residues with sidechain amides (13 Asn and 4 Gln), and 15 charged residues (10 Arg, 2 Lys, and 3 Asp), with a large net charge of +9 (Figure 1A). Using initial conformations of A1-LCD from the previous single-copy simulations,[36] we built an 8-copy model for the dense phase (with a concentration of 3.5 mM) at five NaCl concentrations ranging from 50 to 1000 mM (Figure 1B). Each system was simulated in four replicates for 1 μs each. All the results reported here are averages over the four replicate simulations. From the same initial configuration with very few inter-chain contacts, the systems expand slightly at 50 mM NaCl (Figure 1C) but condense noticeably at 1000 mM NaCl (Figure 1D). At low salt, the protein chains fill the simulation box in two of the three orthogonal directions, with chain configurations rearranging frequently (Supplementary Figure 1). In contrast, at high salt, the chains aggregate into a sphere with much slower chain reconfiguration (correlation time increasing from 30 to 150 ns).

We also quantified the contrast between low and high salt by calculating $D_{max}$, the maximum side length of the rectangular box that parallels the simulation box and circumscribes the multi-chain system. The $D_{max}$ values are above or close to the initial value (~150 Å) at 50 and 300 mM NaCl, but show a clear decrease (to ~125 Å) at 500 and 1000 mM NaCl (Figure 2A). The $D_{max}$ results at 150 mM NaCl are mixed, falling between those at 50 and 300 mM NaCl as expected for the first 400 ns and the last 100 ns but dipping below those at 300 mM for the other half of the simulation time. The latter out-of-order behavior reflects the fact that the multi-chain system can sometimes get stuck in an overly condensed state. Overall, the systems show growing condensation with increasing salt. A small part of the reason for the growing condensation is the compaction of the individual chains. The average radius of gyration ($R_g$) shows a decreasing trend with increasing salt (Figure 2B), which matches the experimental data.[10] Correspondingly, the average number of

intrachain contacts per residue increases slightly, by 4%, when the salt concentration is increased from 50 mM to 1000 mM (Figure 2C). However, the main driver of the condensation is inter-chain interactions, with inter-chain contacts per residue increasing by 22% over the same salt range. Clearly, high salt induces A1-LCD condensation, with an increased number of interactions between protein chains. Below we present the molecular mechanisms for these effects.

**Ions selectively bind to backbone and sidechain sites to neutralize the net charge of A1-LCD**

The large net charge of A1-LCD implies significant electrostatic repulsion between chains. Potentially salt ions can neutralize the net charge. To investigate ion-protein binding, we calculated radial distribution functions (RDFs) of $Cl^-$ and $Na^+$ around polar groups of A1-LCD. At 1000 mM NaCl, the RDFs of $Cl^-$ show a strong 1$^{st}$ peak at 3.2 Å around Arg and Lys sidechain nitrogens and a moderate 1$^{st}$ peak around the Gln and Asn sidechain nitrogens and the Ser sidechain oxygen (Supplementary Figures 2A). Each Arg sidechain often coordinates two $Cl^-$ ions simultaneously, but each Lys sidechain coordinates only one $Cl^-$ ion. A 2$^{nd}$ peak, at ~5 Å, is also observed around Arg and Lys sidechain nitrogens. Of the remaining polar groups, only the $Cl^-$ RDFs around the Tyr sidechain oxygen and the backbone nitrogen show a weak 1$^{st}$ peak (Supplementary Figures 2B). We used cutoffs of 4 and 6.4 Å, respectively, to define 1$^{st}$-shell and 2$^{nd}$-shell $Cl^-$ binding. On a per-residue basis, Arg and Lys sidechains coordinate the most 1$^{st}$-shell $Cl^-$ ions, reaching ~0.25 ions per residue (Figure 3A, left panel). In comparison, each Gln, Asn, or Ser residue, on average, coordinates ~0.05 $Cl^-$ ions. Given the large numbers of Arg and Ser residues in the A1-LCD sequence, these two residue types coordinate the most 1$^{st}$-shell $Cl^-$ ions, 21.6 and 8.9, respectively, in the 8-chain system at 1000 mM NaCl. Although the RDF around backbone nitrogens has only a weak 1$^{st}$ peak, given their large number (131 per chain), they actually coordinate 14.1, or the second most 1$^{st}$-shell $Cl^-$ ions. Among these 14.1 $Cl^-$ ions, 57% are coordinated with Gly residues. A large part of this high percentage is due to the enrichment of Gly (39% of all residues) in the A1-LCD sequence, but Gly is additionally favored for its lack of sidechain, which allows the close approach of ions to the backbone.

$Na^+$ shows a very strong preference for the Asp carboxyl in 1$^{st}$-shell coordination, with a peak RDF value of 12.5 at 2.2 Å (Supplementary Figure 3A). Each Asp sidechain carboxyl

typically coordinates a single $Na^+$ ion, usually in a bifurcated geometry. In addition, $Na^+$ shows a strong preference in 1st-shell coordination with Asn and Gln sidechain amide oxygens and the backbone carbonyl oxygen as well as a moderate preference with the Ser sidechain oxygen. A 2nd peak, at ~4.2 Å, is also observed in the $Na^+$ RDF around the Asp carboxyl. Of the remaining polar groups, only a weak 1st peak is seen in the RDF around the Tyr sidechain oxygen (Supplementary Figure 3B). We used cutoffs of 3 and 5.4 Å, respectively, to define 1st-shell and 2nd-shell $Na^+$ binding. On a per-residue basis, the Asp sidechain coordinates the most 1st-shell $Na^+$ ions, reaching 0.22 ions per residue (Figure 3A, right panel). The per-residue $Na^+$ ion number reduces to ~0.06 for Asn and Glu sidechain oxygens and further to 0.03 for the backbone oxygen and Ser sidechain oxygen. Again, due to their large number, backbone oxygens coordinate a very large number, 30.5, of 1st-shell $Na^+$ in the 8-chain system at 1000 mM NaCl. This number dwarfs the counterparts for sidechains, the largest of which are 7.8, 5.3, and 4.6, respectively, for Asn, Asp, and Ser. For coordination with the backbone, similar to the case with $Cl^-$, 55% of the 30.5 $Na^+$ ions involve Gly residues, again reflecting the fact that this amino acid allows the close approach of ions to the backbone. On the other hand, the largest number of 1st-shell $Cl^-$ ions are coordinated with Arg sidechains but the largest number of 1st-shell $Na^+$ ions are coordinated with backbone carbonyls. Whereas each Arg sidechain often coordinates two $Cl^-$ ions, multiple backbone carbonyls often coordinate a single $Na^+$ ion (see below).

In Figure 3B, we display the total numbers of 1st-shell $Cl^-$ and $Na^+$ ions in the 8-chain systems as a function of NaCl concentration. Both the 1st-shell $Cl^-$ and $Na^+$ ions increase with increasing NaCl concentration, and $Cl^-$ ions always outnumber $Na^+$ ions. The difference remains almost constant, with around 6 more 1st-shell $Cl^-$ ions than 1st-shell $Na^+$ ions. This difference is not enough to neutralize the total charge, +72, on the protein chains. However, when 2nd-shell ions are also included, the excess of bound $Cl^-$ ions over bound $Na^+$ ions grows quickly with increasing NaCl concentration. Correspondingly, the net charge of the system reduces to only +8 at 1000 mM NaCl (Figure 3C), which may be completely neutralized by ions beyond the second shell. Net charge repulsion explains the expansion of the chains in the simulations at 50 mM NaCl (Figure 1C) and the absence of phase separation at this low salt concentration.[10] The protein net charge is largely neutralized by 1st- and 2nd-shell ions at high salt; hence the protein chains condense (Figure 1D) and phase separation is readily observed.[10]

**Ions act as bridges between protein chains to drive condensation**

In addition to charge neutralization, we suspected that ions could also fortify intermolecular interactions by bridging between proteins, similar to the role played by ATP molecules in driving phase separation of positively charged IDPs.[33] Indeed, we found that $Cl^-$ has a tendency to bind with Arg and other sidechains from multiple chains and likewise, $Na^+$ has a tendency to bind with backbone carbonyls and sidechain oxygens from multiple chains (Figure 4A).

To quantify this tendency, we calculated the number of bridging $Cl^-$ or $Na^+$ ions, i.e., those that bind (both 1$^{st}$- and 2$^{nd}$-shell) to residues on more than one A1-LCD chain (Figure 4B). Close to 20% of all 1$^{st}$- and 2$^{nd}$-shell ions bridge between A1-LCD chains. For both $Cl^-$ and $Na^+$, the average number of bridging ions increases with increasing salt, but the pace of increase is much greater for $Na^+$ than for $Cl^-$, commensurate with the trend shown by the total number of bound ions of each type (Figure 3B). The number of bridging ions is 4.1 for $Cl^-$ and only 0.7 for $Na^+$ in the 8-chain system at 50 mM NaCl, and increases to 24.4 and 12.0, respectively, at 1000 mM NaCl. The greater fold change of bridging $Na^+$ ions (18-fold, vs 6-fold for $Cl^-$) is also apparent when we break the bridging ions according to the number of A1-LCD chains being bridged (Figure 4C). For $Cl^-$, the curves plotting the ion count against the number of bridged chains are close to each other among the different NaCl concentrations, but the counterparts for $Na^+$ are more spread out.

These disparate effects of salt concentration on chain bridging by $Cl^-$ and $Na^+$ can be explained by the difference in coordination properties between the two ion types presented above. $Cl^-$ strongly prefers Arg sidechains and, even at low salt, occupies a large number of sites lined by them, of which ~20% are bridging sites. However, there is a relatively limited supply of Arg sidechains (a total of 80 in the 8-chain system) and hence the fold change in bridging $Cl^-$ ions upon salt increase is somewhat tempered. In contrast, although $Na^+$ prefers Asp sidechains, there are very few of those in the system; instead, $Na^+$ predominantly binds to backbone carbonyls. As the latter binding is relatively weak, the number of bridging $Na^+$ ions is very small at low salt. However, since there is a large supply of backbone carbonyls (a total of 1048 in the 8-chain system), at high salt, $Na^+$ ions bind to a portion of these backbone carbonyls and bridge A1-LCD chains. Consequently, at low salt, chain bridging is dominated by $Cl^-$ ($Na^+$ only 14% of bridging

ions), but at high salt, $Na^+$ becomes more even (33% of bridging ions) with $Cl^-$ in bridging A1-LCD chains. An important reason for the latter is $Na^+$ coordination by backbone carbonyls, especially those of Gly residues (Figure 4A).

**Salt also contributes to condensation indirectly by strengthening π-type interactions**

As noted above, the number of inter-chain interactions increases by 22% when the NaCl concentration increases from 50 mM to 1000 mM. While this result could be accounted for by the two direct salt effects presented so far, i.e., charge neutralization and chain bridging, which act to condense A1-LCD, there are additional factors. A breakdown of inter-chain sidechain interactions into different types reveals that when the salt concentration is increased from 50 to 1000 mM, the number of salt bridges per chain actually decreases by 7%, while the numbers of π-π, cation-π, and amino-π interactions increase by 37%, 27%, and 21%, respectively (Figure 5A). That is, as the A1-LCD is condensed at high salt, there is an overall increase in inter-chain interactions, but there is also a redistribution of these interactions among the different types. At increasing salt, more π-types of interactions are formed while fewer salt bridges are formed, suggesting a strengthening of the former interactions but a weakening of the latter.

The weakening of salt bridges by salt can be understood as ions can compete with the salt-bridge partners for coordination (Supplementary Figures 2A and 3A). Indeed, at 1000 mM NaCl, cationic and anionic partners in a salt bridge are often found to also coordinate $Cl^-$ and $Na^+$, respectively (Figure 5B). By contrast, π-π interactions are hardly affected by ion competition (Figure 5C), as Tyr has only a weak ability to coordinate $Cl^-$ and $Na^+$ (Supplementary Figures 2B and 3B) and Phe completely lacks this ability. In comparison, one partner in both cation-π and amino-π interactions can potentially suffer from ion competition (Supplementary Figures 2A and 3A), which may explain why the increases in cation-π and amino-π interactions at high salt are not as large as the counterpart in π-π interactions.

For π-types of interactions, instead of a weakening mechanism through competition, salt may exert a strengthening mechanism by drawing water away from the interaction partners (Figure 5D). We calculated the RDFs of water around Tyr sidechains that form π-types of interactions and found decreases in water density when the salt concentration is increased from 50 to 1000 mM

(Figure 5E and Supplementary Figure 4A-C). As a control, no decrease in water density is seen around Asp sidechains that form salt bridges (Supplementary Figure 4D). Water can interfere with and weaken π-types of interactions; by drawing water away from the interaction partners, high salt strengthens these interactions and thereby indirectly contributes to condensation.

## Discussion

We have shown in atomistic detail the actions of ions in the condensation of A1-LCD over a wide range of NaCl concentrations. The MD simulations reveal that NaCl has both direct and indirect effects in driving phase separation. The first direct effect is to neutralize the net charge of A1-LCD and thereby attenuate net charge repulsion. The second direct effect is to bridge between protein chains and thereby fortify intermolecular interaction networks. In addition, high salt strengthens π-types of interactions by drawing water away from the interaction partners, thereby also indirectly driving phase separation. The net result is that, while phase separation of A1-LCD is prevented by net charge repulsion at low salt, it is enabled at intermediate salt through charge neutralization and chain bridging by ions. The drive for phase separation becomes even stronger at high salt, where π-types of interactions are strengthened.

These findings broaden our understanding of the roles of charges and ions in phase separation. That high net charge is a suppressive factor is highlighted by the strong effect of A1-LCD charge mutations on $C_{sat}$.[29] Here we have shown that this suppressive action can be countered by the addition of salt, which exerts both direct and indirect effects. One of these direct effects, i.e., neutralization of net charge, can be treated by a Debye-Hückel potential in coarse-grained simulations.[30] However, our all-atom explicit-solvent simulations have revealed not only an additional direct effect, i.e., bridging between protein chains, but also an indirect effect, i.e., strengthening of π-type interactions. Krainer et al.[19] observed a reentrant salt effect on the phase separation of IDPs, and attributed the reemergence of phase separation at high salt to strengthened π-type and hydrophobic interactions that overcompensate weakened electrostatic attraction. Their conclusion was based on the salt dependences of the potentials of mean force calculated for pairs of sidechains of various types. Instead of a single pair of sidechains, our simulations are on multiple copies of protein chains. We show that, at high salt, the number of salt bridges is reduced while

the numbers of π-types of interactions are elevated in the multi-chain system. The simulations further reveal that high salt achieves the latter effect by drawing water away from π-interaction partners.

The present work puts us in a position to paint a unified picture of salt dependences of homotypic phase separation (Figure 6A, B and Table 1). The salt dependence that is most often reported is screening, where salts weaken the electrostatic attraction between protein chains and thereby suppress phase separation.[10-17] The reentrant salt dependence reported by Krainer et al.[19] can be seen as an extension of the screening scenario, whereby high salt overcompensates the screening effect by strengthening π-type and hydrophobic interactions and leads to reemergence of phase separation. The high net charge scenario represented by A1-LCD is similar to the reentrant scenario at high salt but differs from it at low salt, where phase separation is prevented by net charge repulsion.[10,20-25,27] In this class of salt dependence, a certain amount of salt is required to start phase separation. For A1-LCD, this minimum salt is ~100 mM NaCl.[10] The recombinant mussel foot protein-1 (RMFP-1) presents an extreme example, which has a net charge of +24 over a sequence length of 121 and requires up to 700 mM NaCl to begin phase separation.[21] The fourth class of salt dependence is a variation of the preceding one; here the net charge is low and no significant net charge repulsion is expected, so the protein can phase separate even without salt. For example, FUS-LCD has a low net charge of -2 and phase separates without salt.[26] The difference between the high and low net charge scenarios is well captured by the phase-separation behaviors of TDP43-LCD at two pHs.[27] At pH 7, this protein has a relatively low net charge of +5 and phase separates without salt; the salt dependence thus belongs to the low net charge class. When pH is lowered to 4, the six His residues in the purification tag become positively charged, raising the net charge to +11; now phase separation requires 300 mM NaCl and the salt dependence switches to the high net charge class.

We can not only rationalize the four distinct classes of sat dependence but also start to predict them from the amino-acid composition of the protein (Figure 6C and Table 1). The foregoing physical understanding suggests three determinants of salt dependence class: (1) the total number of charged residues, which determines the contribution of electrostatic interactions to the drive for phase separation and the importance of salt screening; (2) the net charge, which determines the magnitude of net charge repulsion; and (3) the total number of aromatic residues,

which determines whether phase separation reemerges at high salt. We predict that the screening class occurs when the charged content is high but the net charge and aromatic content are low (Figure 6C). The other three classes of salt dependence all require a high aromatic content. For the reentrant class, the increase in aromatic content is the only difference from the screening class. For the high net charge class, the net charge obviously has to be high, but that could also mean at least a moderately high charged content. Finally the low net charge class is predicted when the net charge is low but no bias is required of the charged content. The amino-acid compositional data in Table 1 validate these predictions. For example, of the 16 proteins in the classes of salt dependence that call for a high aromatic content, 11 (or 68%) actually have this feature (aromatic content > an 8% threshold). In contrast, of the 9 proteins in the class of salt dependence (i.e., "screening") that calls for a low aromatic content, only 2 (or 22%) have an aromatic content above the threshold. In the latter two cases it remains to be tested whether phase separation would reemerge at much higher salt (and thereby resulting in a reclassification to reentrant). Likewise, of the 9 proteins in the class of salt dependence (i.e., "high net charge") that calls for a high net charge, 6 (or 67%) actually have this feature (net charge > a 6% threshold). In contrast, of the 16 proteins in the classes of salt dependence that call for a low net charge, none has a net charge above the threshold. Lastly, of the 14 proteins in the classes of salt dependence that call for a high charge content, 10 (or 71%) actually have this feature (charged content > a 20% threshold). In comparison, of the 11 proteins in the classes of salt dependence that do not require a high charge content, only 2 (or 18%) have a charge content above the threshold.

To conclude, salts regulate intermolecular interactions in biomolecular condensates in a variety of ways, but the net effect on phase separation can be placed into four distinct types (Figure 6A, B). For homotypic condensates, salt effect types are predictable from the protein amino-acid composition. Salts also exert significant effects on heterotypic condensates;[8,18] the conclusions drawn here on homotypic condensates may prove instructive for heterotypic condensates. The fact that different IDPs respond to salts differently raises interesting questions on phase separation inside cells. For example, a fluctuation in intracellular salt concentration may promote the phase separation of some IDPs and suppress the phase separation of other IDPs. If two IDPs co-phase separate or form heterotypic condensates, salt fluctuations may change the protein composition of condensates and the relative contributions of the individual proteins to phase separation. Lastly, we note that the atomistic details of ion coordination to A1-LCD backbone or sidechain groups are

reminiscent of those observed in other systems, in particular channels and transporters for $Na^+$ and $Cl^-$.[37-39]

## Computational Methods

**Molecular dynamics simulations**. MD simulations were performed using AMBER 18[40] with ff14SB force field[41] for the protein and TIP4P-D for water.[42] The initial configuration of the 8-chain system was constructed using A1-LCD conformations from previous single-copy simulations.[36] Specifically, 4 copies with different conformations were placed in a rectangular box, positioned with minimal inter-chain contacts within 3.5 Å. This 4-copy subsystem was duplicated to form the initial configuration of the 8-chain system (Figure 1B). The protein chains were solvated in a box with dimensions of 182 Å × 146 Å × 164 Å. For each desired salt concentration (50, 150, 300, 500, or 1000 mM), an appropriate number of water molecules were randomly selected and replaced with $Cl^-$ and $Na^+$ ions; excess $Cl^-$ was added to neutralize the system. The total number of atoms was ~500,000 for the 8-chain system at each salt concentration.

After energy minimization in sander (2000 steps of steepest descent and 3000 steps of conjugate gradient), each system was heated to 300 K over 100 ps with a 1 fs timestep, under constant NVT using the Langevin thermostat[43] with a 3.0 $ps^{-1}$ damping constant. The simulation was then continued in four replicates at constant NPT for 1 μs with a 2 fs timestep. Pressure was regulated using the Berendsen barostat[44] with a coupling constant of 2.0 ps. All simulations were run on GPUs using *pmemd.cuda*.[45] Bond lengths involving hydrogens were constrained using the SHAKE algorithm.[46] Long-range electrostatic interactions were treated by the particle mesh Ewald method.[47] A cutoff distance of 10 Å was used for the nonbonded interactions. Frames were saved every 200 ps and the last 700 ns was used for analysis.

**Data analysis.** $D_{max}$ was calculated using the minmax function in VMD.[48] The differences between the maximum and minimum values of $x$, $y$, and $z$ coordinates of all protein atoms were obtained; the largest of the three difference values was taken as $D_{max}$. Radius of gyration ($R_g$) was calculated using the radgyr function in CPPTRAJ.[49] For inter- and intrachain contacts per residue, the number of other residues in contact with a given residue was found using the distance mask function in CPPTRAJ with a cutoff of 6 Å between heavy atoms. Inter-chain contacts per chain were found in

a similar way, and were broken into interaction types based on the residue types of the interaction partners. To characterize chain reconfiguration dynamics, the autocorrelation function of the chain end-to-end distance (Cα-Cα distance between the first and last residues) was calculated. After averaging over the 8 chains and then over 4 replicate simulations at each NaCl concentration, the autocorrelation function was fit to an exponential function; the time constant of the fit was taken to be the reconfiguration time.

Radial distribution functions (RDFs) for ions around protein atoms were calculated in CPPTRAJ using the radial command. These RDF plots were used to select cutoffs for $1^{st}$- and $2^{nd}$-shell ion binding; these cutoffs were 4.0 and 6.4 Å, respectively, for $Cl^-$ and 3.0 and 5.4 Å, respectively, for $Na^+$. The number of $1^{st}$-shell or $1^{st}$- and $2^{nd}$-shell ions interacting with N and O atoms in a given sidechain type, the backbone, or the 8 chains together was calculated using CPPTRAJ. Ions were considered bridging if they interacted with two or more chains (based on $2^{nd}$-shell cutoffs) at the same time. Those interacting with an exact number of chains (e.g., 3) were identified when the same ion was found in the interaction lists of that many chains.

RDFs for water molecules around Tyr residues were calculated using VMD. Only Tyr residues that interact with specific residue types (within 6 Å of the 6-carbon ring) were selected: the partner residues were Phe (6-carbon ring; for π-π), Arg and Lys (sidechain N atoms; for cation-π), or Gln and Asn (sidechain N atoms; for amino-π). As a control, PRDFs for water were also calculated around Asp sidechain oxygens that interact with Arg and Lys sidechain nitrogens.

## Acknowledgment

This work was supported by National Institutes of Health Grant GM118091.

## References

(1) Mitrea, D. M.; Cika, J. A.; Stanley, C. B.; Nourse, A.; Onuchic, P. L.; Banerjee, P. R.; Phillips, A. H.; Park, C.-G.; Deniz, A. A.; Kriwacki, R. W. Self-interaction of NPM1

modulates multiple mechanisms of liquid–liquid phase separation. *Nature Communications* **2018,** *9*, 842.

(2) Protter, D. S. W.; Parker, R. Principles and Properties of Stress Granules. *Trends Cell Biol* **2016,** *26*, 668-679.

(3) Das, S.; Lin, Y. H.; Vernon, R. M.; Forman-Kay, J. D.; Chan, H. S. Comparative Roles of Charge, Pi, and Hydrophobic Interactions in Sequence-Dependent Phase Separation of Intrinsically Disordered Proteins. *Proc Natl Acad Sci U S A* **2020,** *117*, 28795-28805.

(4) Dignon, G. L.; Best, R. B.; Mittal, J. Biomolecular Phase Separation: From Molecular Driving Forces to Macroscopic Properties. *Annu Rev Phys Chem* **2020,** *71*, 53-75.

(5) Zhou, H. X.; Kota, D.; Qin, S.; Prasad, R. Fundamental Aspects of Phase-Separated Biomolecular Condensates. *Chem Rev* **2024**, doi:10.26434/chemrxiv-22024-m26494x26432.

(6) Baldwin, R. L. How Hofmeister ion interactions affect protein stability. *Biophys J* **1996,** *71*, 2056-2063.

(7) Zhou, H. X.; Pang, X. Electrostatic Interactions in Protein Structure, Folding, Binding, and Condensation. *Chem. Rev.* **2018,** *118*, 1691-1741.

(8) Farag, M.; Borcherds, W. M.; Bremer, A.; Mittag, T.; Pappu, R. V. Phase separation of protein mixtures is driven by the interplay of homotypic and heterotypic interactions. *Nature Communications* **2023,** *14*, 5527.

(9) Hazra, M. K.; Levy, Y. Cross-Talk of Cation−π Interactions with Electrostatic and Aromatic Interactions: A Salt-Dependent Trade-off in Biomolecular Condensates. *J Phys Chem Lett* **2023,** *14*, 8460-8469.

(10) Martin, E. W.; Thomasen, F. E.; Milkovic, N. M.; Cuneo, M. J.; Grace, C. R.; Nourse, A.; Lindorff-Larsen, K.; Mittag, T. Interplay of folded domains and the disordered low-complexity domain in mediating hnRNPA1 phase separation. *Nucleic Acids Res* **2021,** *49*, 2931-2945.

(11) Tsang, B.; Arsenault, J.; Vernon, R. M.; Lin, H.; Sonenberg, N.; Wang, L.-Y.; Bah, A.; Forman-Kay, J. D. Phosphoregulated FMRP Phase Separation Models Activity-Dependent Translation through Bidirectional Control of mRNA Granule Formation. *Proceedings of the National Academy of Sciences* **2019,** *116*, 4218-4227.

(12) Reed, E. H.; Hammer, D. A. Redox sensitive protein droplets from recombinant oleosin. *Soft Matter* **2018,** *14*, 6506-6513.

(13) Wei, M. T.; Elbaum-Garfinkle, S.; Holehouse, A. S.; Chen, C. C.; Feric, M.; Arnold, C. B.; Priestley, R. D.; Pappu, R. V.; Brangwynne, C. P. Phase behaviour of disordered proteins underlying low density and high permeability of liquid organelles. *Nat Chem* **2017,** *9*, 1118-1125.

(14) Strom, A. R.; Emelyanov, A. V.; Mir, M.; Fyodorov, D. V.; Darzacq, X.; Karpen, G. H. Phase separation drives heterochromatin domain formation. *Nature* **2017,** *547*, 241-245.

(15) Brady, J. P.; Farber, P. J.; Sekhar, A.; Lin, Y. H.; Huang, R.; Bah, A.; Nott, T. J.; Chan, H. S.; Baldwin, A. J.; Forman-Kay, J. D.et al. Structural and hydrodynamic properties of an intrinsically disordered region of a germ cell-specific protein on phase separation. *Proc Natl Acad Sci U S A* **2017,** *114*, E8194-E8203.

(16) Zhang, H.; Elbaum-Garfinkle, S.; Langdon, E. M.; Taylor, N.; Occhipinti, P.; Bridges, A. A.; Brangwynne, C. P.; Gladfelter, A. S. RNA Controls PolyQ Protein Phase Transitions. *Mol Cell* **2015,** *60*, 220-230.

(17) Berry, J.; Weber, S. C.; Vaidya, N.; Haataja, M.; Brangwynne, C. P. RNA transcription modulates phase transition-driven nuclear body assembly. *Proc Natl Acad Sci U S A* **2015,** *112*, E5237-5245.

(18) Galvanetto, N.; Ivanović, M. T.; Chowdhury, A.; Sottini, A.; Nüesch, M. F.; Nettels, D.; Best, R. B.; Schuler, B. Extreme dynamics in a biomolecular condensate. *Nature* **2023,** *619*, 876-883.

(19) Krainer, G.; Welsh, T. J.; Joseph, J. A.; Espinosa, J. R.; Wittmann, S.; de Csillery, E.; Sridhar, A.; Toprakcioglu, Z.; Gudiskyte, G.; Czekalska, M. A.et al. Reentrant liquid condensate phase of proteins is stabilized by hydrophobic and non-ionic interactions. *Nat Commun* **2021,** *12*, 1085.

(20) Muschol, M.; Rosenberger, F. Liquid–liquid phase separation in supersaturated lysozyme solutions and associated precipitate formation/crystallization. *J Chem Phys* **1997,** *107*, 1953-1962.

(21) Kim, S.; Yoo, H. Y.; Huang, J.; Lee, Y.; Park, S.; Park, Y.; Jin, S.; Jung, Y. M.; Zeng, H.; Hwang, D. S.et al. Salt Triggers the Simple Coacervation of an Underwater Adhesive When Cations Meet Aromatic pi Electrons in Seawater. *ACS Nano* **2017,** *11*, 6764-6772.

(22) Dao, T. P.; Kolaitis, R. M.; Kim, H. J.; O'Donovan, K.; Martyniak, B.; Colicino, E.; Hehnly, H.; Taylor, J. P.; Castaneda, C. A. Ubiquitin Modulates Liquid-Liquid Phase Separation of UBQLN2 via Disruption of Multivalent Interactions. *Mol Cell* **2018,** *69*, 965-978 e966.

(23) Le Ferrand, H.; Duchamp, M.; Gabryelczyk, B.; Cai, H.; Miserez, A. Time-Resolved Observations of Liquid-Liquid Phase Separation at the Nanoscale Using in Situ Liquid Transmission Electron Microscopy. *J Am Chem Soc* **2019,** *141*, 7202-7210.

(24) Agarwal, A.; Rai, S. K.; Avni, A.; Mukhopadhyay, S. An intrinsically disordered pathological prion variant Y145Stop converts into self-seeding amyloids via liquid-liquid phase separation. *Proc Natl Acad Sci U S A* **2021,** *118*.

(25) Otis, J. B.; Sharpe, S. Sequence Context and Complex Hofmeister Salt Interactions Dictate Phase Separation Propensity of Resilin-like Polypeptides. *Biomacromolecules* **2022,** *23*, 5225-5238.

(26) Burke, K. A.; Janke, A. M.; Rhine, C. L.; Fawzi, N. L. Residue-by-Residue View of In Vitro FUS Granules that Bind the C-Terminal Domain of RNA Polymerase II. *Mol Cell* **2015,** *60*, 231-241.

(27) Babinchak, W. M.; Haider, R.; Dumm, B. K.; Sarkar, P.; Surewicz, K.; Choi, J. K.; Surewicz, W. K. The role of liquid-liquid phase separation in aggregation of the TDP-43 low-complexity domain. *J Biol Chem* **2019,** *294*, 6306-6317.

(28) Martin, E. W.; Holehouse, A. S.; Peran, I.; Farag, M.; Incicco, J. J.; Bremer, A.; Grace, C. R.; Soranno, A.; Pappu, R. V.; Mittag, T. Valence and patterning of aromatic residues determine the phase behavior of prion-like domains. *Science* **2020,** *367*, 694-699.

(29) Bremer, A.; Farag, M.; Borcherds, W. M.; Peran, I.; Martin, E. W.; Pappu, R. V.; Mittag, T. Deciphering how naturally occurring sequence features impact the phase behaviours of disordered prion-like domains. *Nat Chem* **2022,** *14*, 196-207.

(30) Tesei, G.; Lindorff-Larsen, K. Improved Predictions of Phase Behaviour of Intrinsically Disordered Proteins by Tuning the Interaction Range. *Open Res. Eur.* **2023,** *2*, 94.

(31) Lin, Y.-H.; Forman-Kay, J. D.; Chan, H. S. Sequence-Specific Polyampholyte Phase Separation in Membraneless Organelles. *Phys Rev Lett* **2016,** *117*, 178101.

(32) Garaizar, A.; Espinosa, J. R. Salt dependent phase behavior of intrinsically disordered proteins from a coarse-grained model with explicit water and ions. *J Chem Phys* **2021,** *155*. (acccessed 6/6/2024).

(33) Kota, D.; Prasad, R.; Zhou, H. X. Adenosine Triphosphate Mediates Phase Separation of Disordered Basic Proteins by Bridging Intermolecular Interaction Networks. *J Am Chem Soc* **2024,** *146*, 1326-1336.

(34) Zhang, Y.; Prasad, R.; Su, S.; Lee, D.; Zhou, H.-X. Amino Acid-Dependent Material Properties of Tetrapeptide Condensates. *bioRxiv* **2024**, DOI:10.1101/2024.05.14.594233 10.1101/2024.05.14.594233. (acccessed 2024-05-15).

(35) Rekhi, S.; Garcia, C. G.; Barai, M.; Rizuan, A.; Schuster, B. S.; Kiick, K. L.; Mittal, J. Expanding the molecular language of protein liquid–liquid phase separation. *Nat Chem* **2024**, DOI:10.1038/s41557-024-01489-x 10.1038/s41557-024-01489-x.

(36) Dey, S.; MacAinsh, M.; Zhou, H. X. Sequence-Dependent Backbone Dynamics of Intrinsically Disordered Proteins. *J Chem Theory Comput* **2022,** *18*, 6310-6323.

(37) Leisle, L.; Lam, K.; Dehghani-Ghahnaviyeh, S.; Fortea, E.; Galpin, J. D.; Ahern, C. A.; Tajkhorshid, E.; Accardi, A. Backbone amides are determinants of Cl(-) selectivity in CLC ion channels. *Nat Commun* **2022,** *13*, 7508.

(38) Mancusso, R.; Gregorio, G. G.; Liu, Q.; Wang, D. N. Structure and mechanism of a bacterial sodium-dependent dicarboxylate transporter. *Nature* **2012,** *491*, 622-626.

(39) Mita, K.; Sumikama, T.; Iwamoto, M.; Matsuki, Y.; Shigemi, K.; Oiki, S. Conductance selectivity of Na(+) across the K(+) channel via Na(+) trapped in a tortuous trajectory. *Proc Natl Acad Sci U S A* **2021,** *118*.

(40) Case, D. A.; Ben-Shalom, I. Y.; Brozell, S. R.; Cerutti, D. S.; Cheatham, T. E.; Cruzeiro, V. W. D.; Darden, T. A.; Duke, R. E.; Ghoreishi, D.; Gilson, M. K. AMBER 2018, University of California, San Francisco. **2018**.

(41) Maier, J. A.; Martinez, C.; Kasavajhala, K.; Wickstrom, L.; Hauser, K. E.; Simmerling, C. ff14SB: Improving the Accuracy of Protein Side Chain and Backbone Parameters from ff99SB. *J Chem Theory Comput* **2015,** *11*, 3696-3713.

(42) Piana, S.; Donchev, A. G.; Robustelli, P.; Shaw, D. E. Water dispersion interactions strongly influence simulated structural properties of disordered protein states. *J Phys Chem B* **2015,** *119*, 5113-5123.

(43) Pastor, R. W.; Brooks, B. R.; Szabo, A. An analysis of the accuracy of langevin and molecular dynamics algorithms. *Mol Phys* **1988,** *65*, 1409-1419.

(44) Berendsen, H. J. C.; Postma, J. P. M.; van Gunsteren, W. F.; DiNola, A.; Haak, J. R. Molecular dynamics with coupling to an external bath. *J Chem Phys* **1984,** *81*, 3684-3690.

(45) Salomon-Ferrer, R.; Gotz, A. W.; Poole, D.; Le Grand, S.; Walker, R. C. Routine Microsecond Molecular Dynamics Simulations with AMBER on GPUs. 2. Explicit Solvent Particle Mesh Ewald. *J Chem Theory Comput* **2013,** *9*, 3878-3888.

(46) Ryckaert, J. P.; Ciccotti, G.; Berendsen, H. J. C. Numerical integration of the cartesian equations of motion of a system with constraints: molecular dynamics of n-alkanes. *J Comput Phys* **1977,** *23*, 327-341.

(47) Essmann, U.; Perera, L.; Berkowitz, M. L.; Darden, T.; Lee, H.; Pedersen, L. G. A smooth particle mesh Ewald method. *J Chem Phys* **1995,** *103*, 8577-8593.

(48) Humphrey, W.; Dalke, A.; Schulten, K. VMD: visual molecular dynamics. *J Mol Graph* **1996,** *14*, 33-38, 27-38.

(49) Roe, D. R.; Cheatham, T. E., 3rd. PTRAJ and CPPTRAJ: Software for Processing and Analysis of Molecular Dynamics Trajectory Data. *J Chem Theory Comput* **2013,** *9*, 3084-3095.

Table 1. Correlation between class of salt dependence and amino-acid composition

| Protein | Length | Charges (+/-/net)[b] | Aromatic[d] | Salt (mM) | Ref |
|---|---|---|---|---|---|
| | | Screening | | | |
| hnRNPA1 | 314 | **42 / 34** / 8 | **33** | NaCl 50-300 | 10 |
| FMRP-LCD | 188 | **37 / 28**[e] / 9 | 6 | NaCl 0-150 | 11 |
| Oleo30G | 139 | 15 / 12 / 3 | 7 | NaCl 35-280 | 12 |
| LAF-1 | 708 | **86 / 88** / -2 | 55 | NaCl 125-400 | 13 |
| LAF-1 RGG | 191 | **28 / 22** / 6 | 14 | NaCl 125-300 | 13 |
| HP1α | 206 | **33 / 41** / -8 | 14 | NaCl 25-150 | 14 |
| Ddx4 | 236 | **32 / 36** / -4 | **22** | NaCl 100-500 | 15 |
| PolyQ | 729 | 38 / 34 / 4 | 35 | NaCl 0-150 | 16 |
| FIB-1 | 352 | **55 / 34** / 21 | 24 | NaCl 50-250 | 17 |
| | | Reentrant | | | |
| FUS | 526 | 51 / 37 / 14 | **52** | KCl 50-2700 | 19 |
| TDP-43 | 414 | **40 / 44** / -4 | **36** | KCl 50-2700 | 19 |
| Brd4 | 1362 | **175 / 150** / 25 | 48 | KCl 50-2150 | 19 |
| Sox2 | 317 | 34 / 21 / 13 | 19 | KCl 50-2150 | 19 |
| A11 | 505 | **51 / 50** / 1 | **41** | NaCl 22.5-500 | 19 |
| | | High net change | | | |
| A1-LCD | 131 | 12 / 3 / **9** | **18** | NaCl 50-300 | 10 |
| Lysozyme[a] | 129 | **17 / 9** / **8** | **12** | NaCl 514-1198 | 20 |
| RMFP-1 | 121 | 24 / 0 / **24** | **24** | NaCl 100-500 | 21 |
| UBQLN2 | 624 | 31 / 40 / -9 | 22 | NaCl 100-300 | 22 |
| UBQLN2 (450-624) | 175 | 4 / 8 / -4 | 5 | NaCl 50-200 | 22 |
| HBP-2 (pH 5.5) | 193 | **30**[c] **/ 13** / **17** | **20** | NaCl 50-500 | 23 |
| Prp-LCD | 122 | 11 / 1 / **10** | **11** | NaCl 150-750 | 24 |
| $RLP3_8$ | 120 | 12 / 8 / 4 | 8 | NaCl 0-2000 | 25 |
| TDP43-LCD (pH 4) | 148 | 14[c] / 3 / **11** | **12** | NaCl 0-300 | 27 |
| | | Low net charge | | | |
| FUS-LCD | 136 | 0 / 2 / -2 | **20** | NaCl 0-250 | 26 |
| TDP43-LCD (pH 7) | 148 | 8 / 3 / 5 | **12** | NaCl 0-300 | 27 |

[a]Single-domain folded protein.

[b]Charges are listed as the number of positively (R and K, including H when specifically indicated) or negatively (D and E) charged residues or net charge.

[c]H is treated as positively charged at the low pH condition.

[d]Aromatic residues are W, Y, and F.

[e]High contents of charged residues, net charges, and aromatic residues are indicated by bold letters, with thresholds at 20%, 6%, and 8%, respectively, when measured as percentages of the sequence length.

**Figure Captions**

Figure 1. Amino-acid sequence of A1-LCD and molecular dynamics simulations of its condensation. (A) Amino-acid sequence. (B) First and (C, D) last frames from 1-μs simulations of the 8-chain systems at low and high salt. In all figures, $Cl^-$ or $Na^+$ ions are represented by green and magenta spheres, respectively.

Figure 2. Salt effects on A1-LCD condensation and inter-chain interactions. (A) $D_{max}$ values, averaged over four replicates, as a function of simulation time. (B) Radii of gyration ($R_g$) from small-angle X-ray scattering[10] and from MD simulations. Dashed curves are drawn to guide the eye. (C) Average number of inter- or intra-chain contacts per residue at each salt concentration. Dashed lines are drawn to show trends.

Figure 3. Levels of ion binding at different NaCl concentrations. (A) Number of 1$^{st}$-shell ions, with (darker colors; tick marks on the left vertical axis) and without (lighter colors; tick marks on the right vertical axis) normalization by the number of residues of a given amino-acid type, at 1000 mM NaCl. (B) Total number of 1$^{st}$-shell only or 1$^{st}$- and 2$^{nd}$-shell ions. (C) Net charge of the system with 1$^{st}$- and 2$^{nd}$-shell ions included.

Figure 4. Bridging ions. (A) Examples of chain bridging by $Cl^-$ and $Na^+$; $Cl^-$ ions are coordinated to Arg and other sidechains whereas $Na^+$ ions are coordinated to both backbone carbonyls (including from Gly) and sidechain oxygens. (B) Average number of $Cl^-$ or $Na^+$ ions engaged in bridging between A1-LCD chains. (C) Average number of ions bound in 1$^{st}$- and 2$^{nd}$-shell sites lined by a given number of A1-LCD chains.

Figure 5. Indirect effects of ions on different types of interactions. (A) Number of inter-chain contacts per chain for each interaction type. Bars from left to right correspond to increasing salt concentrations (50, 150, 300, 500, and 1000 mM). Dashed lines are drawn to show trends. (B) An inter-chain salt bridge, with ion coordination by the partner sidechains. (C) An inter-chain π-π interaction, free of ion coordination. (D) Schematic showing a π-π interaction facilitated by high salt, via drawing water away from the interaction partners. (E) Radial distribution functions of water around Tyr residues that interact with Phe, Arg, Lys, Gln, and Asn. Lower values at high salt demonstrate water withdrawal.

Figure 6. Four classes of salt dependence and their prediction from amino-acid composition. (A) Salt dependences of liquid-liquid phase separation (LLPS). (B) Charge-charge and π-type interactions and their regulation by salt. (a) Significant Charge-charge attraction. (b) Screening of charge-charge attraction by salt. (c) Strengthening of π-type interactions by high salt. (d) Repulsion due to high net charge. (C) Distinctions of the four classes of salt dependence by three determinants: charged content ("Chg"), net charge ("Net"), and aromatic content ("Aro").

**A**

```
1    GSMASASSSQ RGRSGSGNFG GGRGGGFGGN DNFGRGGNFS  40
41   GRGGFGGSRG GGGYGGSGDG YNGFGNDGSN FGGGGNYNNQ  80
81   SSNFGPMKGG NFGGRSSGPY GGGGQYFAKP RNQGGYGGSS  120
121  SSSSYGSGRR F                                 131
```

**B**

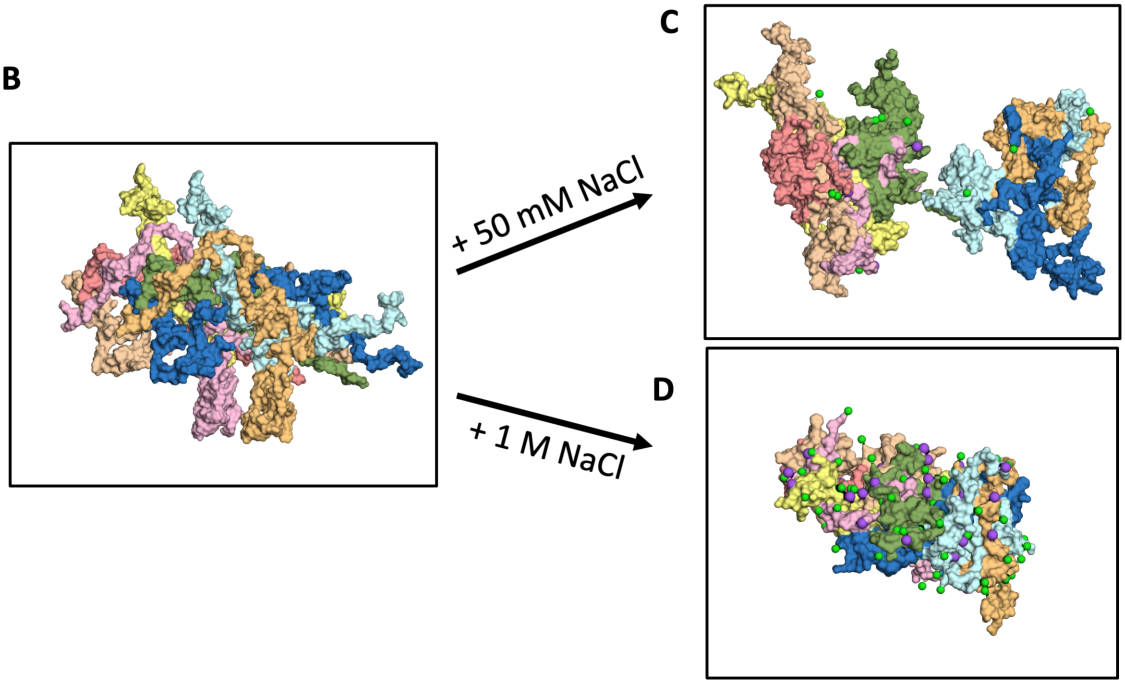


Figure 1

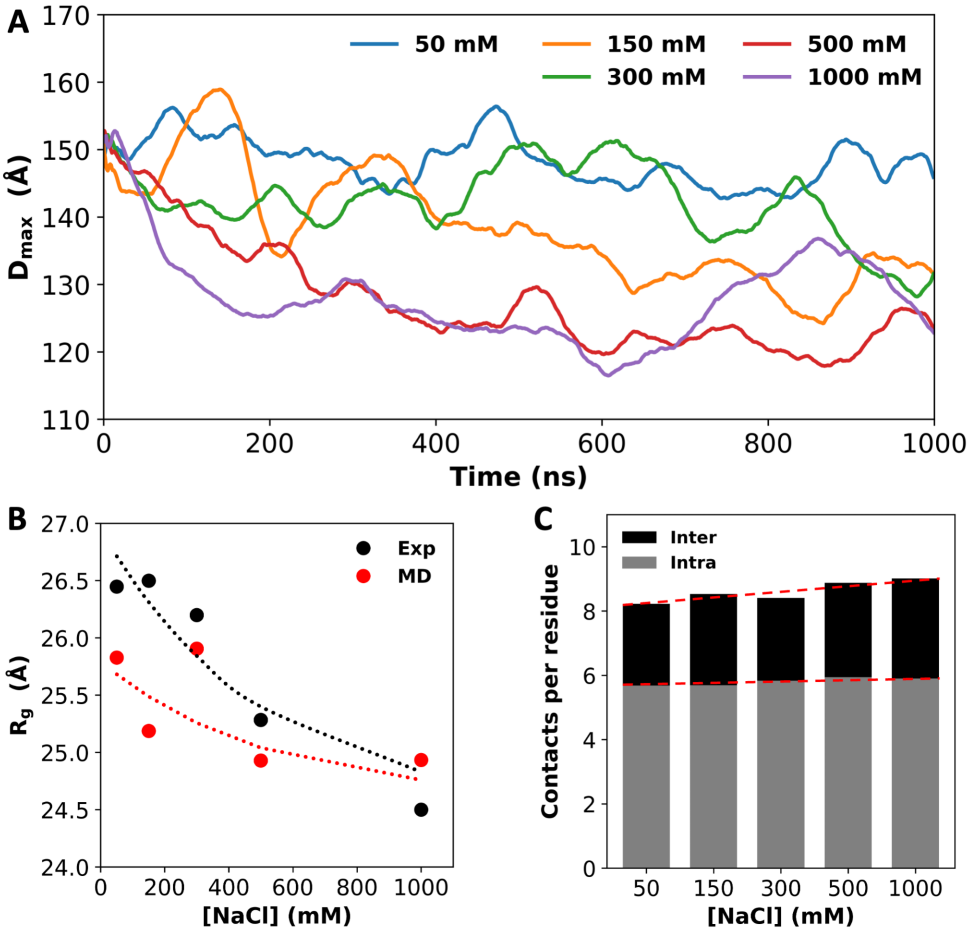
A
50 mM
150 mM
500 mM
300 mM
1000 mM
$D_{max}$ (Å)
Time (ns)
B
Exp
MD
$R_g$ (Å)
[NaCl] (mM)
C
Inter
Intra
Contacts per residue
[NaCl] (mM)

Figure 2

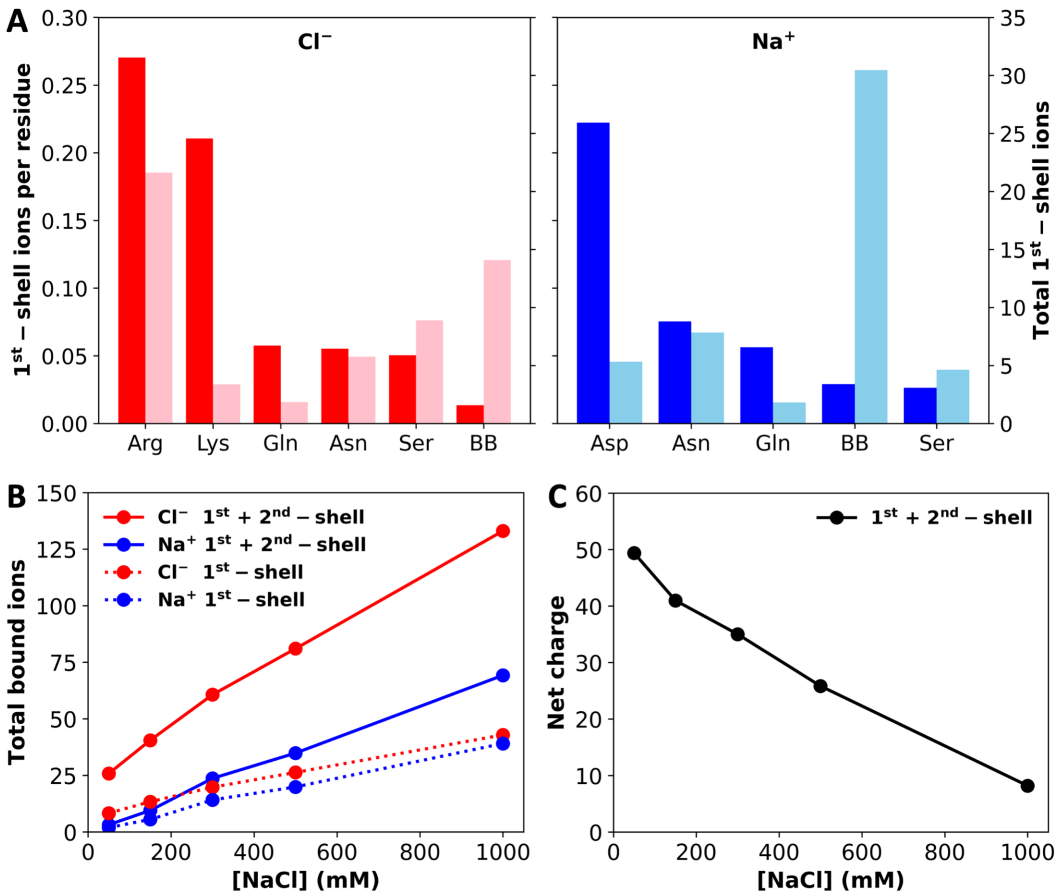
A
Cl⁻
Na⁺
1st – shell ions per residue
Total 1st – shell ions
Arg
Lys
Gln
Asn
Ser
BB
Asp
Asn
Gln
BB
Ser
B
Cl⁻ 1st + 2nd – shell
Na⁺ 1st + 2nd – shell
Cl⁻ 1st – shell
Na⁺ 1st – shell
Total bound ions
[NaCl] (mM)
C
1st + 2nd – shell
Net charge
[NaCl] (mM)

Figure 3

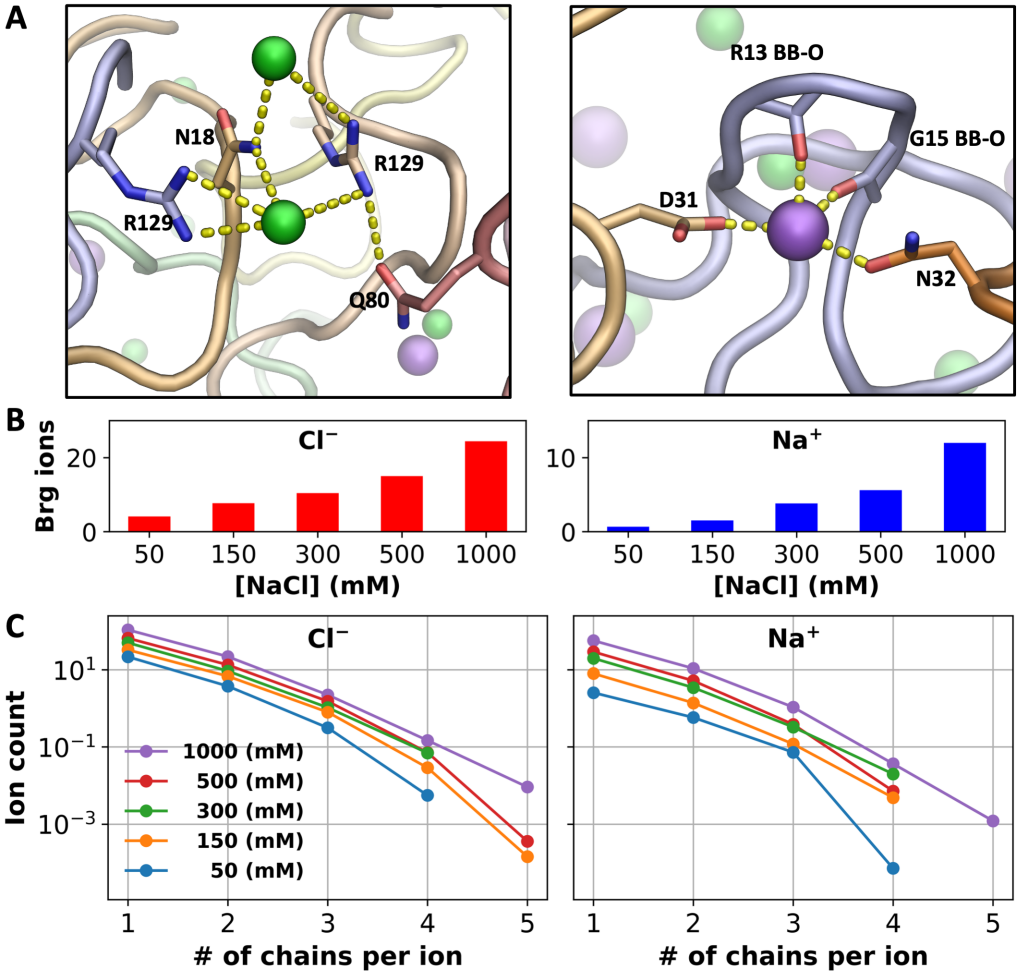
A
N18
R129
R129
Q80
R13 BB-O
G15 BB-O
D31
N32
B
Brg ions
Cl⁻
Na⁺
[NaCl] (mM)
[NaCl] (mM)
C
Ion count
Cl⁻
Na⁺
1000 (mM)
500 (mM)
300 (mM)
150 (mM)
50 (mM)
# of chains per ion
# of chains per ion

Figure 4

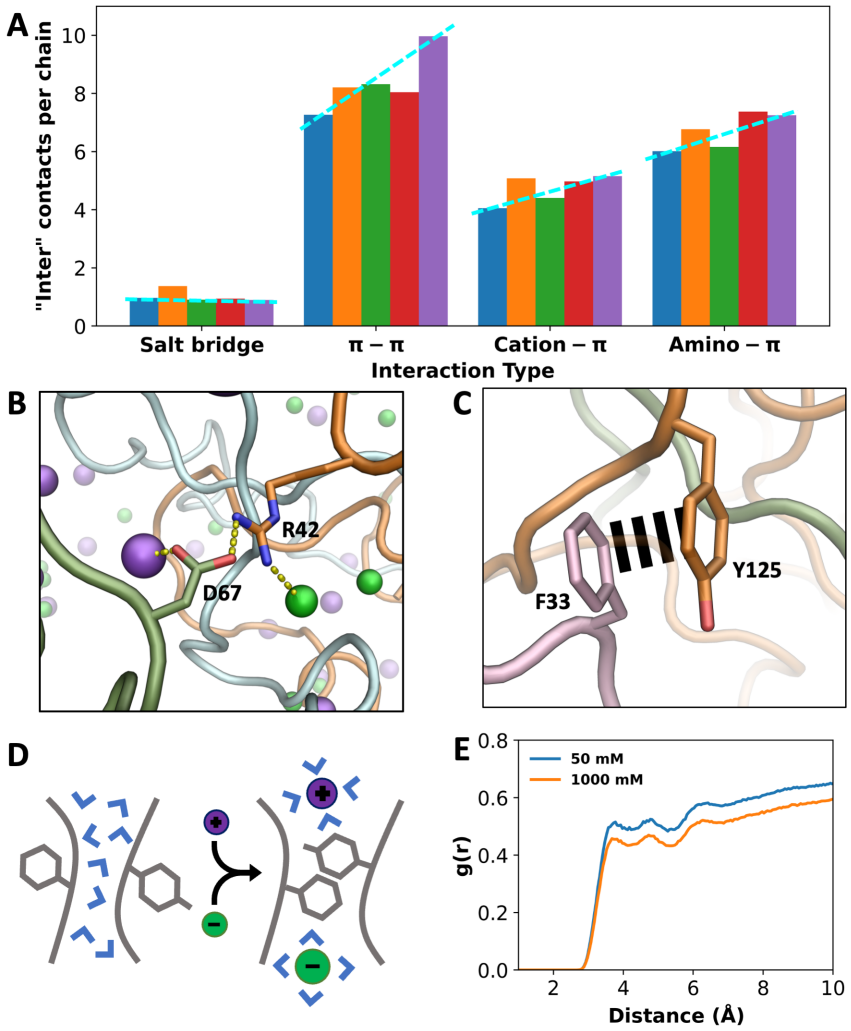
A
"Inter" contacts per chain
0
2
4
6
8
10
Salt bridge
π – π
Cation – π
Amino – π
Interaction Type
B
R42
D67
C
F33
Y125
D
E
50 mM
1000 mM
g(r)
0.0
0.2
0.4
0.6
0.8
2
4
6
8
10
Distance (Å)

Figure 5

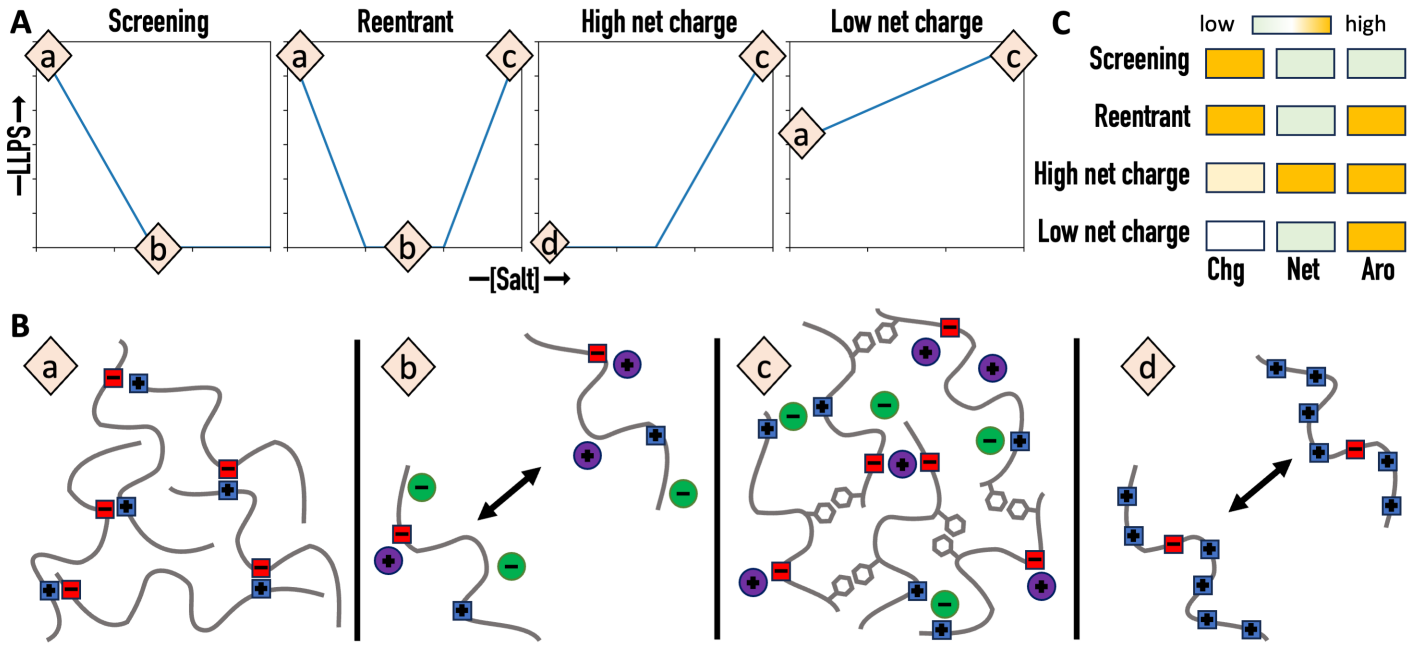
A
Screening
Reentrant
High net charge
Low net charge
a
b
c
d
—LLPS→
—[Salt]→
C
low
high
Screening
Reentrant
High net charge
Low net charge
Chg
Net
Aro
B

Figure 6